Biogeosciences Discuss., 9, 4819–4852, 2012
www.biogeosciences-discuss.net/9/4819/2012/
doi:10.5194/bgd-9-4819-2012

Biogeosciences Discussions

Glacial-interglacial variability in ocean oxygen and phosphorus in a global biogeochemical model

V. Palastanga[1], **C. P. Slomp**[1], **and C. Heinze**[2]

[1]Department of Earth Sciences-Geochemistry, Faculty of Geosciences, Utrecht University, Budapestlaan 4, Utrecht, 3584 CD, The Netherlands
[2]Geophysical Institute, University of Bergen, Allegaten 70, 5007, Bergen, Norway

Received: 28 March 2012 – Accepted: 2 April 2012 – Published: 19 April 2012

Correspondence to: V. Palastanga (v.palastanga@uu.nl)

Published by Copernicus Publications on behalf of the European Geosciences Union.

Abstract

The importance of particulate organic carbon and phosphorus (P) delivered from shelves on open ocean productivity, oxygen, and reactive P burial during glacial times has been assessed using a biogeochemical ocean model of the carbon (C), P and iron cycles. The model shows that in simulations of the Last Glacial Maximum (LGM) without any inputs of terrigenous material from shelves there is a moderate increase in productivity (+5 %) and mean deep water oxygen (+29 %) relative to the preindustrial simulation. However, when the input of terrigenous particulate organic C and P is considered as an additional forcing in the LGM simulation, ocean productivity increases by 46 %, mean deep water oxygen concentration decreases by 20 %, and the global rate of reactive P burial is 3 times over the preindustrial value. The associated pattern of negative oxygen anomalies at 1000 m induces a deepening of the Atlantic and Indian Ocean oxygen minimum (OMZ), while in the Pacific Ocean the OMZ is shifted to the eastern basin north of the Equator relative to preindustrial times. In addition, negative trends in oxygen extend globally below 2000 m depth, though their magnitude is rather weak, and in particular bottom waters remain above suboxic levels. Changes in dust deposition can be responsible for positive trends in reactive P burial as simulated at the LGM in open ocean regions, notably over the Southwest Atlantic and Northwest Pacific; on the other hand, inputs of terrigenous material from shelves cause an increase in P burial over the continental slope and rise regions which accounts for 47 % of the total reactive P burial change. Although the glacial-interglacial trends in P burial in our model compare well with the available observations, this study highlights the need of much more core records of C and P in open ocean settings.

1 Introduction

Phosphorus (P) is an essential nutrient in marine biogeochemistry and is believed to limit primary productivity on geological time scales (Tyrrell, 1999). Burial in sediments

BGD
9, 4819–4852, 2012

is the only removal pathway for P in the marine environment. In the present-day ocean, a major proportion of the total burial of reactive P takes place on continental margins (>50 %, Ruttenberg, 1993; Filippelli, 1997). Sea level fall during glacial periods may have led to a reduction of this continental margin sink and enhanced erosion of shelf material and transport to the deep sea. The increased transfer of nutrients and carbon from shelves to the open ocean likely had an impact on open ocean biogeochemistry. For example, the inventory of P in the open ocean, primary productivity and the drawdown of CO_2 from the atmosphere may have all increased. This so-called shelf-nutrient hypothesis was first brought forward by Broecker (1982) and has been revived in various recent studies of marine P cycling in the ocean (Filippelli et al., 2007; Tamburini and Föllmi, 2009; Tsandev et al., 2010).

Using geochemical records from deep ocean sites in the Southern Ocean and the equatorial Pacific, Filippelli et al. (2007) make the case that there was an increase in P burial toward the end of glacials and the beginning of interglacials. Based on simple model calculations, they argue that a redistribution of P from the marginal to the deep-sea sink and enhanced biological productivity could explain the observed excess P sedimentation. Based on an analysis of P burial in sediment cores from the Ocean Drilling Programme (ODP), in contrast, Tamburini and Föllmi (2009) show that there was a slight decrease in P burial at many deep-sea locations in glacial times (on average 8 %). These authors suggest that the P released from shelves during glacials remained in the water column and enhanced the P inventory and primary productivity in the ocean.

Several box model studies of carbon and P dynamics in the ocean confirm that sea level fall could lead to an increase in the deep ocean phosphate inventory during glacial stages that could potentially impact primary productivity (Wallmann, 2003; Tsandev et al., 2008). Model scenarios that, besides sea level change, include multiple glacial-interglacial cycles and changes in ocean circulation lead to simulated export production rates for glacial periods that are lower or similar to interglacial values (Tsandev et al., 2008). If, however, shelf erosion and rerouting of particulate material from shelves

BGD
9, 4819–4852, 2012

through canyons is included, primary production in the glacial ocean increases relative to interglacials (Tsandev et al., 2010). Under these conditions, deep-sea oxygen levels can drop significantly, promoting recycling of P relative to organic carbon from sediments (e.g. Algeo and Ingall, 2007), which may contribute to a further decline in oxygen (Wallmann, 2003; Tsandev et al., 2010).

Several proxy data suggest that deep waters were indeed less oxygenated during glacial periods over large areas of the three ocean basins (François et al., 1997; Mangini et al., 2001; Sirocko et al., 2000; Jaccard et al., 2009). Bradtmiller et al. (2010) hypothesized that lower deep water oxygen concentrations inferred from the enrichment of authigenic uranium concentrations in sediments of the equatorial Pacific could have been part of a basin scale phenomenon, involving a deepening of the oxygen minimum zone (OMZ) and larger storage of organic C in the sediment. Because low oxygen conditions enhance the recycling of P relative to C from organic matter (e.g. Algeo and Ingall, 2007; Slomp and Van Cappellen, 2007), increased organic matter input and burial may not always be recorded in the burial record of total P (e.g. Tsandev et al., 2010). However, the sediment P speciation in dysaerobic settings may change with authigenic Ca-P and Fe-oxide bound P both becoming less important as a burial sink as reported for North Atlantic sediments during Heinrich events 4 and 5 in the last glacial period (Tamburini et al., 2002). Note however that such P speciation results should be viewed with caution given their possible alteration due to long-term diagenesis and post-sampling artifacts (e.g. Kraal et al., 2009, 2010).

Besides changes in P dynamics, enhanced supply of iron (Fe) rich dust during glacial periods likely affected primary productivity and marine biota and may have impacted global atmospheric pCO_2 drawdown (e.g. Bopp et al., 2003; Maher et al., 2010). While the oceanic Fe cycle is the topic of numerous modeling studies (Aumont et al., 2003; Parekh et al., 2005; Moore and Braucher, 2008), there is currently no ocean biogeochemical model for long-term simulations that allows the assessment of coupled changes in the marine cycles of P and Fe and that includes sediment processes.

BGD
9, 4819–4852, 2012

In this study, we expand a biogeochemical ocean model developed for the C, P and silicon cycles (Palastanga et al., 2011) with the Fe cycle to investigate the regional and global scale trends in C export production, ocean oxygen and marine P cycling linked to variability on glacial-interglacial time scales. A specific goal is to test the response in deep water oxygenation and redox dependent P burial to an increase in the delivery of particulate C and P from shelves to the open ocean at glacial times. Our work builds on the box modeling work of Tsandev et al. (2010), but instead of assessing the average response of the global ocean as a whole, we use an ocean biogeochemical model which also allows an assessment of possible regional changes. The model we use is a new version of the Hamburg Oceanic Carbon Cycle (HAMOCC) model for long-term integrations (Heinze et al., 1999, 2003) that incorporates a full description of the sedimentary P cycle and a new component for the oceanic Fe cycle. The model is forced by either the glacial or interglacial fields of ocean circulation and atmospheric dust deposition, and the differences between these simulations are analyzed. Subsequently, we discuss the sensitivity of the results of the LGM simulation to varying inputs of particulate organic C (POC) and particulate inorganic P (PP) from aerially exposed shelves during glacial periods. Our results show that the input of POC and P from shelves in a glacial setting can have a significant impact on productivity, deep water oxygen and, in contrast to what was suggested in previous modeling work, on burial of reactive P in the global open ocean. This work also highlights the regional variability in the response of the marine P cycle to glacial-interglacial change.

2 Methods

2.1 Model description

We use the model of Palastanga et al. (2011), which is itself a version of the HAMOCC model (Heinze et al., 1999, 2003), expanded to include anaerobic degradation of organic matter in the sediment and a full description of the sedimentary P cycle.

BGD
9, 4819–4852, 2012

The physical model is based on the annual mean flow of the Hamburg Large Scale Geostrophic ocean circulation model (Maier-Reimer et al., 1993), with a horizontal resolution of 3.5° × 3.5° and 11 layers in the water column. In this section, we briefly describe the modifications made in the model to incorporate a description of the oceanic Fe cycle. A detailed description of the original model formulation can be found in Heinze et al. (2003) and Palastanga et al. (2011).

In the model, it is assumed that all dissolved iron (Fe) is in free inorganic form, and thus bioavailable. Both phosphate (PO_4) and Fe can limit the rate of POC export production. The annual rate of POC export is determined by the minimum between the uptake rate of PO_4 and Fe assuming Michaelis Menten kinetics, an approach similar to that in the model of Archer and Johnson (2000). We assume a uniform half saturation constant for Fe (K_{fe}) equal to 0.003 nM (Archer and Johnson, 2000). The ratio of Fe fixation to organic matter (Fe:C) is 4 μmol : 1 mol (Parekh et al., 2005). Because of POC mineralization, Fe is released back to the water column at this fixed ratio following the same parameterization used for POC in the original model.

Fe is removed from the water column by scavenging (e.g. precipitation and adsorption) onto sinking particles. Scavenging of Fe is modeled as a first order process, with the rate being equal to a rate constant (k_{scav}) times the difference between the actual Fe concentration and an apparent 'solubility' constant of 0.6 nM (Johnson et al., 1997; Archer and Johnson, 2000). The latter is aimed to represent the observed relatively constant concentrations of total Fe in deep waters, possibly a consequence of Fe complexation. Scavenging is also limited by the particle load in the water column (Aumont et al., 2003; Parekh et al., 2005). Therefore, similar to Aumont et al. (2003) we assume that the scavenging rate constant (k_{scav}) is given by a minimum uniform rate (0.01 yr^{-1}) plus a particle dependent rate set as 1.8 l μmol^{-1} yr^{-1} times the sum of the concentration of the sinking POC, opal, calcite and clay. It is assumed that only 10 % of the total scavenged Fe goes to the sinking flux of particulate Fe (Moore and Braucher, 2008), while the rest redissolves and is artificially removed from the water column.

BGD
9, 4819–4852, 2012

The sources of Fe in the model are dust and sediments. We use the annual mean dust deposition fields from Mahowald et al. (2006), assuming that Fe is 1.5 wt % of dust, with a constant solubility in seawater of 1 %. Although the aerosol Fe solubility is not a well-constrained parameter in the ocean yet (Baker and Croot, 2008), the value used here is in agreement with the observed global average Fe solubility, i.e. 1–2 %, and is aimed to simulate realistic concentrations of Fe and PO_4 in the surface ocean. The release of Fe from sediments is prescribed using the parameterization from Moore and Braucher (2008), where it is assumed to be a function of the POC flux to the seafloor. However, we adjust the correlation used by Moore and Braucher (2008) to a release of 0.2 µmolFe m^{-2} day^{-1} for each mmolC m^{-2} day^{-1} settling into the ocean floor, thus reducing the importance of the sedimentary source. By this choice the model simulates reasonable concentrations of surface Fe in open ocean areas which are affected by offshore advection of Fe from margin sediments. The sedimentary flux of Fe is finally weighted by the actual ocean bathymetry from the ETOPO2 version 2.0 database to account for the release of Fe from sediments in shelf regions not properly resolved by the model bathymetry (Aumont and Bopp, 2006).

Different from previous models, here we describe the input of particulate Fe into the ocean (in the form of highly reactive Fe or Fe-oxides) and its cycling in sediments. Model values for dust and river fluxes of Fe-oxides are set consistent with mass balance estimates from Raiswell (2006). The total input of highly reactive Fe from dust is calculated from the atmospheric dust deposition fields of Mahowald et al. (2006), which results in a net atmospheric input of 1.95 Tg yr^{-1}, and in particular, an input of 1.45 Tg yr^{-1} over the ocean region with depths > 1000 m. The total input of Fe-oxides from rivers to the ocean area with depths < 1000 m is assumed to be 2.8 Tg yr^{-1}. Global estimates for the export of Fe-oxides from continental margins to the deep ocean are highly uncertain at 4 ± 12 Tg yr^{-1} (Raiswell, 2006), thus, as a first approximation to this flux, we assume that 1 Tg yr^{-1} of Fe-oxides from rivers is homogeneously deposited over the ocean surface area with depths between $1000 < z < 3500$ m. Inputs of Fe-oxides from hydrothermal activity and icebergs are neglected in this study, though the

BGD
9, 4819–4852, 2012

latter could be an important source of highly reactive Fe into the open ocean (Raiswell, 2006). A complete description of the global inputs of total P and Fe in the model is given in Table 1.

The sediment module in the model is expanded to incorporate a simplified description of sedimentary Fe dynamics. The flux of sinking Fe-oxides from dust and rivers is not subject to further dissolution in the water column and sets the upper boundary condition for the input of particulate Fe into the sediment. The model simulates transport, mixing and burial of Fe-oxides as well as porewater diffusion of dissolved Fe. Precipitation of Fe to form Fe-oxides is modeled in the aerobic part of the sediment ($O_2 > 5\,\mu mol\,l^{-1}$) following a bimolecular rate law dependent on the porewater Fe and oxygen concentration (Van Cappellen and Wang, 1996). The rate constant for Fe oxidation is set to $0.5 \times 10^7\,M\,yr^{-1}$ which lies within the range reported in the literature (Van Cappellen and Wang, 1996; Canavan et al., 2006). Reductive dissolution of Fe-oxides is simulated in the anaerobic part of the sediment ($O_2 < 5\,\mu mol\,l^{-1}$) as a first order reaction proportional to the concentration of Fe-oxides, with no threshold concentration for Fe-oxide reduction. The value of the dissolution rate constant is set to $0.025\,yr^{-1}$ by model fitting. Secondary reactions involving Fe are not included; in particular, oxidation of organic matter by Fe-oxide reduction is not considered, which is not unreasonable given the relatively low fluxes of organic matter in the model (Wijsman et al., 2002). In the present approach, the concentration of Fe-oxide bound P (Fe-P) in the sediment is determined by the input, formation, and dissolution of Fe-oxides assuming a globally uniform Fe to P ratio for Fe-P of 20 (Kraal et al., 2010).

2.2 Simulations

Simulations were carried out using either the preindustrial or LGM simulated fields of the annual mean ocean circulation from Winguth et al. (1999) and annual mean dust deposition fluxes from Mahowald et al. (2006). For the preindustrial case (reference run), the model was integrated for 200 kyr, after which the model is very close to equilibrium (Palastanga et al., 2011). To simulate a scenario that represents LGM

BGD
9, 4819–4852, 2012

conditions, the model was run from the reference case solution for a period of 120 kyr using LGM forcings (LGM simulation).

To test the effect of an increase in the delivery of particulate matter from shelves to the open ocean in a LGM scenario, a series of experiments were run as part of a sensitivity analysis (Table 2). As in the present model continental margins are not properly represented (i.e. there are almost no grid points with depths < 200 m), we simulate the fluxes of terrigenous material from shelves as a prescribed input of POC or PP into the model area with depths > 200 m. During interglacial periods, most of this particulate material is trapped on continental margins (Ruttenberg, 1993). Hence, terrigenous fluxes to the open ocean are set to zero in the model reference run. According to Wallmann (2003), the lowering of sea level in glacial periods caused a shift of terrigenous sedimentation from shelves to the continental rise and slope regions (i.e. the ocean area between 200–2000 m water depth). Estimates for the flux of POC delivered to the open ocean from erosion of exposed shelves during glacial times range from 2.3 to 25 $\mathrm{TmolC\,yr^{-1}}$, which represents a total input of 1.2–12.5 $\times 10^5$ TmolC assuming that deposition occurred over a period of 50 kyr, though the timing of the delivery of the POC material to the ocean is not well constrained (Tsandev et al., 2010). On the other hand, Ruttenberg (1993) suggests that a reduction of 50 % in the areal extent of continental margins at glacial maxima could have implied a transfer of reactive P to the open ocean of up to 0.09 $\mathrm{TmolP\,yr^{-1}}$, of which a significant fraction could have been in non-organic form, e.g. authigenic-P. To implement the input of terrigenous C and P in the LGM simulation, first we ran an LGM scenario which includes a flux of POC (and organic P) into the model continental slope and rise regions ($200 < z < 2000$ m, also referred as "margins") equal to 5 $\mathrm{TmolC\,yr^{-1}}$. This rate is chosen assuming that in the model the POC flux is constant over the whole period of integration, thus giving at the end of the simulation a total input of POC equal to 6.0×10^5 TmolC. Second, we ran a simulation of the LGM that considers the input of terrigenous PP into the model margins and no input of terrigenous POC. Since there are almost no constraints on the flux of PP from shelves into the open ocean at glacial times, here we assume a

BGD
9, 4819–4852, 2012

constant flux of 0.02 TmolP yr^{-1}, which is not remobilized in the water column and is eventually deposited into the sediment, with a fractionation for PP equal to 50 % authigenic Ca-P and 50 % Fe-P. Finally, we ran a simulation of the LGM which combines the two above scenarios (i.e. both fluxes of 5.0 Tmol yr^{-1} POC and 0.02 Tmol yr^{-1} PP are added simultaneously over the whole period of integration), and this is referred to as the "full LGM simulation". A description of the global fluxes of P and Fe in the full LGM simulation is given in Table 1. Note that because of enhanced dust deposition at the LGM, the input of dissolved nutrients into the ocean increases, in particular, that of dissolved Fe in the full LGM case is over 2 times its reference value. Also, the input of particulate inorganic P (i.e. Fe-oxide bound P and authigenic Ca-P of atmospheric origin) into the deep ocean area ($z > 2000$ m), and which is eventually deposited into the sediment, increases significantly at the LGM as a consequence of the glacial dust field.

3 Results and discussion

3.1 Preindustrial simulation

Because the dynamics of the Fe cycle were not included in previous versions of the model (Palastanga et al., 2011), here we present a brief description of the most relevant results of the model reference run. The model dissolved Fe at the surface (Fig. 1a) shows high concentrations under the dust plumes in the tropical Atlantic and North Indian Ocean, in the Arctic Ocean and, locally, in continental margin areas, while concentrations are typically low in the Pacific Ocean. A comparison of these simulated large-scale features to a recompilation of global Fe observations from Parekh et al. (2005) indicates reasonable agreement between model and data. However, the model simulates too high concentrations in the eastern equatorial Pacific and in the Southern Ocean, which is probably a consequence of the lack of scavenging for Fe concentrations below 0.6 nM in areas of strong upwelling (Moore and Braucher, 2008). The

BGD
9, 4819–4852, 2012

model distribution of Fe in deep waters (Fig. 1b) is characterized by a uniform value of 0.6 nM in the open ocean, and relatively higher concentrations around continental margins where the influence of the sedimentary Fe source is large. The decrease in deep water Fe concentration with distance from the coast is consistent with observations (Moore and Braucher, 2008), but in general the model Fe concentrations are overestimated in the ocean interior and underestimated in the northeast Pacific (compare to Fig. 1b from Parekh et al., 2005). In addition, while high model scavenging rates are needed to simulate reasonable Fe concentrations near the surface, these induce a very smoothed pattern of deep water Fe, and even in high deposition regions Fe is quickly scavenged below the surface. Other processes not included in the model, such as binding of Fe to organic ligands, seem to be crucial to reproduce the inter-basin gradients of the observed deep water Fe distribution (Parekh et al., 2005).

The annual rate of POC export production predicted by the model (8.96 $Pg\,yr^{-1}$) is in agreement with estimates from other biogeochemical ocean models (e.g. Aumont et al., 2003). Iron limits productivity over most of the Pacific Ocean (with the exception of the northeastern corner of the basin), the Southern Ocean, and off the western South African margin (not shown). Thus, although the model captures the broad pattern of Fe limitation associated with the well-known high nutrient low chlorophyll (HNLC) oceanic regions, it overestimates their extension into the Equatorial Pacific and over the South Pacific subtropical gyre. This is in part related to deficiencies in the model surface PO_4 concentrations which are higher than observations in the equatorial and tropical Pacific due to too high upwelling velocities and "nutrient trapping", a problem of low-resolution particle only models (Heinze et al., 1999; Archer and Johnson, 2000). The excess PO_4 in the tropics is then transferred by lateral advection to subtropical latitudes, causing productivity there to be limited by Fe availability.

Concentrations of Fe-oxides in the sediment (averaged over the bioturbated layer; Fig. 1c) are high in open ocean locations with high rates of atmospheric deposition, such as the tropical and southwest Atlantic and the western Indian Ocean. Vertical profiles of Fe-oxides in the sediment show that reductive dissolution is an important

BGD
9, 4819–4852, 2012

process along continental margins with high rates of POC deposition and anaerobic remineralization (Fig. 2a, b). In contrast, deep-sea settings show net accumulation of Fe-oxides in the sediment, with no recycling of dissolved Fe (Fig. 2c). The sediment Fe-oxide and porewater Fe concentrations simulated for the North Atlantic continental slope (Fig. 2a) are in good agreement with the range of 20 to 40 $\mu mol\,g^{-1}$ Fe and maximum dissolved Fe of 60 $\mu mol\,l^{-1}$ as measured by Slomp et al. (1996). However, while the model porewater profile indicates constant upward diffusion of Fe, observations show a decrease in Fe concentration at depth in the sediment, which is probably caused by Fe monosulfide and pyrite formation, processes that are not included in the model. The global burial rate of Fe predicted by the model ($42.2 \times 10^9\,mol\,yr^{-1}$) is lower than estimates from mass balance calculations that range between 75–$200 \times 10^9\,mol\,yr^{-1}$ (Raiswell, 2006). This is, however, not surprising since in the model the input of Fe-oxides is most likely to be at the lower end of estimates and relevant Fe sources are neglected (Sect. 2.1).

The global distribution of the sedimentary P phases in the model is similar to that simulated by Palastanga et al. (2011) and is therefore not shown., There are a few small differences in the amplitude of the open ocean maxima in authigenic Ca-P and Fe-P, mainly because of the use of a different dust field (Mahowald et al., 2006). In particular, with the new parameterization for Fe-P formation used here, the average concentrations of Fe-P in the sediment ranges between 0.2–1.0 $\mu mol\,g^{-1}$ in the open ocean, whereas larger values are simulated near continental margins. As a consequence, the magnitude of the model Fe-P sink (6 % of total reactive P burial) is lower than estimates from observations in open ocean and continental slope settings (Ruttenberg, 1993; Slomp et al., 1996). Still, the distribution of reactive P burial in the model shows little change relative to previous simulations (Palastanga et al., 2011).

3.2 Comparison between the preindustrial and LGM simulation

The change in POC export production for the LGM simulation relative to the reference run is presented in Fig. 3. Relative to interglacial periods, glacial export production

BGD
9, 4819–4852, 2012

decreases over the tropical Pacific, along the eastern Pacific and South African upwelling margins, and in general at high latitudes due to the glacial sea ice cover. Increases are observed over most of the Atlantic and Indian Ocean basins and over the western North Pacific. When compared to indicators of primary production from the paleoclimatic sediment core record during the LGM (see Fig. 5a from Bopp et al., 2003), the model performs quite well and reproduces most of the observed global trends, with notable exceptions being the eastern equatorial Pacific and the waters off the South African coast. Simulations forced by either the dust or circulation LGM field show that the circulation field is responsible for the spatial distribution and magnitude of the anomalies in productivity at the LGM; nevertheless, the positive trend induced by dust forcing is locally relevant because, for example, it amplifies the anomalies in the central North Pacific and reverses negative trends in the Arabian Sea and the subtropical South Atlantic. The effect of dust (and bioavailable Fe input) in the LGM simulation is also important for atmospheric CO_2 drawdown. While in the LGM simulation forced by circulation alone the global rate of POC export production does not change and pCO_2 drops by merely 4 ppm relative to interglacials, in the LGM simulation using dust forcing alone there is a +7 % increase in global POC export production together with a 20 ppm decrease in pCO_2. When both circulation and dust forcing are considered, the model simulates a +5 % increase in global POC export production (Fig. 4a) and a decrease of 14 ppm in pCO_2. This differs from the modeling study of Bopp et al. (2003), who predicted a global decrease in POC export production of −7 % and a pCO_2 drawdown of 30 ppm in their glacial scenario under full forcings; the discrepancy here is probably due to differences in the LGM circulation field used by the two models.

For the LGM simulation the model predicts an increase in the global mean concentration of PO_4 (+14 %) and oxygen, with the largest simulated changes in oxygen at 1000 m, i.e. the mean deep water oxygen concentration increases from 112 µmol l^{-1} in the reference run to 146 µmol l^{-1} in the LGM case (Fig. 4b, c). Higher glacial oxygen in the model could be related to changes in circulation as well as decreasing temperatures, and hence better oxygen solubility in seawater. The distribution of oxygen

BGD
9, 4819–4852, 2012

anomalies at 1000 m depth (LGM relative to preindustrial; Fig. 5a) shows large positive trends in the eastern tropical South Pacific and the western north Pacific basin, while weak negative trends are simulated over the tropical Indian and Atlantic oceans. This implies that, at the LGM, there is a shallowing of the Pacific OMZ (here defined as [O2] < 25 µmol l^{-1}) from 1000 m deep in the reference case to 700 m deep in the LGM simulation, and the oxygen minimum in the Pacific is constrained to the eastern basin north of the Equator (Fig. 5b). Bottom water oxygen shows minor changes relative to preindustrial, with slightly more oxygenated bottom waters along the northern North Pacific margins and in the eastern equatorial Pacific (not shown).

Changes in sediment reactive P in the LGM simulation (Fig. 6a) largely follow the global-scale trends in POC export production. Therefore, changes in reactive P concentrations are mostly related to anomalies in organic P concentrations over the tropical Indian and Atlantic Ocean and to ocean-wide changes in authigenic Ca-P. The increase in reactive P concentrations simulated in the eastern equatorial Pacific is probably related to a decrease in total sedimentation rates there. Dust forcing alone is responsible for large positive anomalies in sediment reactive P (10 µmol g^{-1}) along the North Pacific and South Atlantic subtropical bands, and in general, for a global positive trend in reactive P concentrations at the LGM. In the LGM simulation, the latter is overcome over the central Pacific basin and the Southern Oceans by large negative anomalies in reactive P induced by the glacial circulation field. Overall, the global rate of reactive P burial in the LGM simulation (0.032 TmolP yr^{-1}) is only 10 % higher than the preindustrial value. Global POC burial also increases by 9 % relative to the reference case, with the largest positive anomalies along the western Atlantic and Indian Ocean margins (not shown). Large positive trends in reactive P burial in the southwest Atlantic and northern North Pacific follow positive anomalies in sedimentation rates caused by enhanced dust deposition; in addition, glacial dust deposition induces a pattern of alternating positive and negative anomalies in reactive P burial along the western tropical Indian Ocean margin (Fig. 6b). Reactive P burial rates are lower in normally high productivity upwelling zones along the eastern Pacific and off South Africa, in the northern North Atlantic,

BGD
9, 4819–4852, 2012

and over the central Pacific and parts of the Southern Oceans. These results highlight that changes in dust input are important in determining regional changes in reactive P burial in the open ocean.

3.3 Sensitivity of the LGM simulation to the input of terrigenous material

3.3.1 LGM scenario with terrigenous POC

In the simulation of the LGM described above the input of terrigenous material from shelves to the open ocean was set to zero. Including a flux of terrigenous POC ($5\,\mathrm{TmolC\,yr^{-1}}$) to the model continental slope and rise regions in the LGM simulation has a significant impact on the deep-water PO_4 and productivity. The model rate of POC export production shows a relative increase of 34 % and the global mean PO_4 concentration increases by almost 2 times over the preindustrial value (Fig. 4a, b). In addition, because of the increase in oxygen demand in deep waters, global mean oxygen and deep-water oxygen show a negative trend relative to preindustrial, although the simulated decrease in oxygen concentrations is small (−4 % at 1000 m depth, Fig. 4c). Reactive P burial increases relative to interglacial times (not shown) reflecting the increase in productivity along continental margins as well as a global increase in water column PO_4; exceptions to this trend lie in regions where productivity significantly decreases at the LGM such as off the eastern Pacific margin and at high latitudes.

3.3.2 LGM scenario with terrigenous PP

We now consider the effect of including a flux of terrigenous PP equal to $0.02\,\mathrm{TmolP\,yr^{-1}}$ in the LGM simulation with no inputs of POC from shelves. Relative to the preindustrial case, the model simulates an increase of 15 % in global POC export production, +37 % in global mean PO_4 concentration, and +17 % in mean deep-water oxygen concentration (Fig. 4a–c). The simulated changes in water column PO_4 and productivity are related to a relative increase in the benthic P flux over the model

BGD
9, 4819–4852, 2012

continental slope and rise regions (+36 % relative to preindustrial). Despite the simulated boost in productivity, the change in deep-sea respiration demand is not enough to overcome the positive trend in deep-water oxygen concentrations induced by the glacial circulation field, and only at abyssal depths negative trends in oxygen are simulated. Because of the direct input of reactive P to margin sediments, burial of reactive P increases significantly over that region, with anomalies of up to 200 µmolP cm^{-2} kyr^{-1} relative to the LGM simulation with no inputs of terrigenous materials (not shown).

3.3.3 Full LGM simulation

With the full LGM simulation, we analyze the combined effects of including the input of both terrigenous POC and PP into the model continental slope and rise regions. Relative to the preindustrial simulation, the model shows a 46 % increase in global export production and a 2.5 times increase in the PO_4 inventory (Fig. 4a, b). Because of the large increase in surface PO_4, POC export production becomes limited by Fe availability over most of the basins (with exception of the high productivity near coastal areas). The global mean oxygen concentration decreases by 12 %, but the largest change in oxygen appears around 1000 m depth (−20 % relative change), where the mean oxygen concentration falls down to 89 µM (Fig. 4c). The distribution of oxygen anomalies at 1000 m (Fig. 5c) shows a predominance of negative anomalies (except over the Pacific basin north of 40° S), with the largest negative trends over the tropical North Atlantic (oxygen anomalies < −100 µM) and the subtropical and western Indian Ocean (oxygen anomalies −70 µM). The pattern of oxygen concentrations at 1000 m shows a deepening of the Atlantic and Indian Ocean OMZ relative to preindustrial times, and the Pacific OMZ is reduced in extension to the northeastern basin (Fig. 5d). Although bottom waters do not reach suboxic levels, bottom water oxygen concentrations along high productivity margins lie within 25–100 µM, which is considerably lower than in the LGM simulation with no inputs of terrigenous materials.

Sediment reactive P shows a considerable increase relative to preindustrial (Fig. 6c). Changes in open ocean areas are caused by an increase in the model sediment

BGD
9, 4819–4852, 2012

authigenic Ca-P concentrations (over 90 % of the total P change), whereas changes in organic P explain the trends along margins at tropical/subtropical latitudes of the Indian and Atlantic Ocean. There is also a significant increase in Fe-P concentrations over the non-reducing margin sediments of the Southern Ocean and the northern North Atlantic. The resulting rate of reactive P burial (0.1 TmolP yr^{-1}) is three times larger than the preindustrial rate. This is consistent with the estimated increase in reactive P burial associated with the loss of about 50 % of the continental margin sink at glacial peaks (Ruttenberg, 1993). Relative to preindustrial conditions, reactive P burial increases everywhere except off the eastern equatorial Pacific coast, in the northern North Atlantic, and in parts of the Southern Oceans (Fig. 6d). As expected, the effect of including the delivery of particulate material from shelves leads to a significant increase in total sedimentation rates and reactive P burial over the continental slope and rise regions, which accounts for 47 % of the total change in reactive P burial.

3.4 Comparison of model results for the LGM to other studies

Records of sedimentary P concentrations and P burial during the last glacial period are still sparse on a global scale (Tamburini and Föllmi, 2009). Here, we present a comparison between the glacial trends in P burial from observations available in the literature and from two LGM scenarios (Table 3). Given the large variation in the reported data, we categorize the trends as “increase”, “decrease”, “no change” and “trend unclear”. In general, the model reproduces the observed trends in open ocean locations well, especially in the Southern Ocean and the eastern tropical Atlantic, where the model also simulates an increase in productivity at glacial times. Reactive P burial in the full LGM simulation is higher than in the LGM simulation but the trends relative to the preindustrial scenario are usually comparable (with the exception of the central equatorial Pacific and the Java plateau). Model-data discrepancies could be related to the fact that transient changes in circulation are not considered in the model (e.g. compare to Tsandev et al., 2010) and to model deficiencies to simulate glacial productivity, for example, in the equatorial Pacific (Bopp et al., 2003). A comparison between model

BGD
9, 4819–4852, 2012

and data near continental margins is difficult due to the coarse resolution of the model. While the model predicts an increase in P burial on the upwelling margin off the western coast of Mexico, Ganeshram et al. (2002) suggests a significant decrease in phosphogenesis and total P burial in these environments. However, the decrease in productivity and P burial simulated along most of the eastern tropical Pacific margin is in agreement with a decline in phosphogenesis, although for the region off the coast of Peru Tamburini and Föllmi (2009) reported an increase in reactive P burial. On the other hand, the model simulates an increase in P burial at locations in the North Indian Ocean that coincides with the positive trends in the data but which is not always in agreement with the timing of the observed peaks (e.g. at a site in the Oman margin reactive P burial peaks at the beginning of glacial periods, Tamburini et al., 2003).

Low oxygen concentrations as observed in the glacial ocean could only be obtained with the model in the full LGM scenario, i.e. when assuming the influx of particulate material from shelves. Specifically, at 1000 m depth the model full LGM scenario predicts large negative oxygen anomalies over the tropical North Atlantic and the subtropical/western Indian Ocean, and positive oxygen anomalies over most of the Pacific Ocean. These anomalies lead to a pattern of well-defined oxygen minima in the three ocean basins, with the position of the Pacific OMZ shifted to the eastern basin north of the Equator. At depths below 1000 m, the model simulates negative trends in oxygen over the three ocean basins (only below 2000 m in the central-eastern tropical Pacific). These modeled trends do not contradict indications from data of less oxygenated deep waters in areas of the tropical Atlantic and subarctic Pacific at glacial peaks (Mangini et al., 2001; Jaccard et al., 2009); still, the magnitude of oxygen anomalies in the model is rather weak, thus oxygen concentrations at e.g. 3000 m depths do not fall below 125 $\mu mol\,l^{-1}$. On the other hand, the model differs from observations that suggest lower oxygen concentrations in the east equatorial Pacific around 2000 m, and in particular, the model does not support the hypothesis of a deepening of the Pacific OMZ during glacial periods (Bradtmiller et al., 2010). However, the increase in oxygen concentrations in the tropical Pacific at the LGM is largely related to the ocean circulation field;

BGD
9, 4819–4852, 2012

because the glacial circulation is better constrained by observations in the Atlantic than in the Pacific Ocean (Winguth et al., 1999), future analysis could test the sensitivity of the results in the tropical Pacific to a different glacial circulation field.

Our results are in agreement with previous box modeling studies that show that the decrease in deep water oxygenation at glacial times only starts to be significant when large amounts of organic shelf material are delivered to the open ocean (Wallmann, 2003). However, while in those models redox-dependent P recycling is pointed as a key mechanism to drive glacial trends in ocean productivity and oxygen (Wallmann, 2003), or in P burial (Tsandev et al., 2010), in the scenarios simulated here bottom water oxygen concentrations are above suboxic levels, thus the feedback from preferential P regeneration from sediments is not yet activated. It should be noted that the estimates for the POC flux from shelves to the deep sea during glaciations, as well as the way in which this flux is implemented in models, are highly uncertain. In addition, there are currently almost no constraints on the anomalous delivery of inorganic P and highly reactive Fe from continental sources to the open ocean at glacial times. For instance, it has been suggested that the flux of Fe-oxides delivered by icebergs could have been 3 times larger at the LGM than at present times, still, the pathways of the iceberg Fe-flux into the open ocean, as well as its potential bioavailability, are unknown (Raiswell et al., 2006). Further data of sediment organic C composition and P speciation in open ocean settings may allow a better assessment of the role of terrigenous material in regulating global ocean productivity and deep water oxygenation during glacial periods.

4 Conclusions and outlook

We use a biogeochemical ocean model of the carbon (C), phosphorus (P) and iron (Fe) cycles to compare the trends in ocean productivity, oxygen, and P cycling at the peak of glacial periods relative to the preindustrial ocean. The model gives a detailed representation of the sedimentary P dynamics, including anaerobic POC remineralization in sediments and redox dependent P burial. However, because of the coarse

BGD
9, 4819–4852, 2012

resolution of the model, the dynamics of continental margins are poorly represented. To simulate glacial scenarios we use simulated fields of ocean circulation and atmospheric dust deposition for the LGM. In addition, fluxes of particulate organic C (POC) and particulate inorganic P (PP) are added to the model continental rise and slope regions ($200 < z < 2000$ m) to simulate erodible particulate matter from shelves which is potentially transferred to the open ocean during sea level low stands.

In the model LGM simulation without any inputs of particulate material from shelves, POC export production increases by 5 % relative to interglacial periods, while the global mean phosphate and deep-water oxygen concentrations increase by 14 % and 29 %, respectively. When the input of terrigenous material is included as an additional forcing in the model LGM scenario, the glacial trends in productivity and global mean phosphate concentration are accentuated, whereas the mean deep water oxygen concentration decreases by −20 % relative to preindustrial times. This suggests that erosion of particulate material from shelves was a prerequisite for the development of low oxygen in the glacial ocean. Dust is an important source of P in sediments in open ocean regions. The LGM simulation using full glacial forcings (circulation, dust, and delivery of particulate material from shelves) shows that relative to interglacial periods the increase in productivity in the tropical Atlantic and Indian Ocean, as well as along the subtropical bands of the South Atlantic and Northwest Pacific, is correlated with positive anomalies in reactive P burial over these open ocean regions. The largest changes in reactive P burial are simulated, though, along the continental slope and continental rise due to the delivery of P from shelves into those regions. On average, the rate of reactive P burial increases 3 times over the preindustrial value, and only in localized ocean areas such as off the equatorial East Pacific coast and at high latitudes of the North Atlantic and Southern Ocean the model simulates a decrease in reactive P burial.

Despite the limitation of our model to represent the dynamics intrinsic to circulation and coastal sea level changes during glacial-interglacial transitions, the model simulations provide new insights into the spatial distribution of deep-water oxygen anomalies during glacial peaks and possible changes in P burial. Additional sediment records of

BGD
9, 4819–4852, 2012

total and reactive P, organic carbon and proxies of water column redox conditions for the open ocean are needed for a further reconstruction of marine P cycling on glacial-interglacial time scales.

Acknowledgements. This is publication DWxxx of the Darwin Center for Biogeosciences and Axxx from the Bjerknes Centre for Climate Research. We also acknowledge funding from the Netherlands Organization for Scientific Research (NWO Vidi grant), from Utrecht University (High Potential grant) and the European Union (European Research Council Starting Grant 278364 to C. P. Slomp)

References

Algeo, T. J. and Ingall, E.: Sedimentary C_{org}:P ratios, paleocean ventilation, and Phanerozoic atmospheric pO_2, Palaeogeogr. Palaeocl., 256, 130–155, 2007. 4822

Archer, D. E. and Johnson, K.: A model of the iron cycle in the ocean, Global Biogeochem. Cy., 14, 269–279, 2000. 4824, 4829

Aumont, O. and Bopp, L.: Globalizing results from ocean in situ iron fertilization studies, Global Biogeochem. Cy., 20, GB2017, doi:10.1029/2005GB002591, 2006. 4825

Aumont, O., Maier-Reimer, E., Blain, S., and Monfray, P.: An ecosystem model of the global ocean including Fe, Si, P colimitations, Global Biogeochem. Cy., 17, 1060, doi:10.1029/2001GB001745, 2003. 4822, 4824, 4829

Bradtmiller, L. I., Anderson, R. F., Sachs, J. P., and Fleisher, M. Q.: A deeper respired carbon pool in the glacial equatorial Pacific ocean, Earth Pl. Sc. Lett., 229, 417–425, 2010. 4822, 4836

Baker, A. R. and Croot, P. L.: Atmospheric and marine controls on aerosol iron solubility in seawater, Mar. Chem., 120, 4–13, doi:10.1016/j.marchem.2008.09.003, 2010. 4825

Bopp, L., Kohfel, K. E., and Le Quéré, C.: Dust impact on marine biota and atmospheric CO2 during glacial periods, Paleoceanography, 18, 1046, doi:10.1029/2002PA000810, 2003. 4822, 4831, 4835

Broecker, W. S.: Glacial to interglacial changes in ocean chemistry, Prog. Oceanogr., 11, 151–197, 1982. 4821

BGD

9, 4819–4852, 2012

Canavan, R. W., Slomp, C. P., Jourabchi, P., Van Cappellen, P., Laverman, A. M., and van den Berg, G. A.: Organic matter mineralization in sediment of a coastal freshwater lake and response to salinization, Geochim. Cosmochim. Ac., 70, 2836–2855, 2006. 4826

Filippelli, G. M.:Controls on phosphorus concentration and accumulation in oceanic sediments, Mar. Geol., 139, 231–240, 1997. 4821

Filippelli, G. M., Latimer, J. C., Murray, R. W., and Flores, J. A.: Productivity records from the Southern Ocean and the equatorial Pacific Ocean: testing the glacial shelf-nutrient hypothesis, Deep-Sea Res., 54, 2443–2452, 2007. 4821

François, R., Altabet, M. A., Yun, E., Sigmans, D. M., Bacon, M. P., Frank, M., Bohrmann, G., Bareille, G., and Labeyrie, L. D.: Contribution of Southern Ocean surface-water stratification to low atmospheric CO_2 concentrations during the last glacial period, Nature, 389, 929–935, 1997. 4822

Ganeshram, R. S., Pedersen, T. F., Calvert, S. E., and François, R.: Reduced nitrogen fixation in the glacial ocean inferred from changes in marine nitrogen and phosphorus inventories, Nature, 415, 156–159, 2002. 4836

Heinze, C., Maier-Reimer, E., Winguth, A. M. E., and Archer, D.: A global oceanic sediment model for long-term climate studies, Global Biogeochem. Cy., 13, 221–250, 1999. 4823, 4829

Heinze, C., Hupe, A., Maier-Reimer, E., Dittert, N., and Ragueneau, O.: Sensitivity of the marine Si cycle for biogeochemical parameter variations, Global Biogechem. Cy., 17, 1086, doi:10.1029/2002GB001943, 2003. 4823, 4824

Jaccard, S. L., Galbraith, E. D., Sigman, D. M., Haug, G. H., François, R., Pedersen, T. F., Dulski, P., and Thierstein, H. R.: Subarctic Pacific evidence for a glacial deepening of the oceanic respired carbon pool, Earth Pl. Sc. Lett., 277, 156–165, 2009. 4822, 4836

Johnson, K. S., Gordon, R. M., and Coale, K. H.: What controls dissolved iron concentrations in the world ocean? Mar. Chem., 57, 137–161, 1997. 4824

Kraal, P., Slomp, C. P., Forster, A., Kuypers, M. M. M., and Sluijs, A.: Pyrite oxidation during sample storage determines phosphorus fractionation in carbonate? poor anoxic sediments, Geochim. Cosmochi. Acta, 73, 3277–3290, 2009. 4822

Kraal, P., Slomp, C. P., Forster, A., and Kuypers, M. M. M.: Phosphorus cycling from the margin to abyssal depths in the proto-Atlantic during oceanic anoxic event 2, Palaeogeogr. Palaeocl., 295, 42–54, 2010. 4822, 4826

BGD
9, 4819–4852, 2012

Maher, B. A., Prospero, J. M., Mackie, D., Gaiero, D., Hesse, P. P., and Balkanski, Y.: Global connections between aeolian dust, climate and ocean biogeochemistry at the present day and at the last glacial maximum, Earth Sc. Rev., 99, 61–97, 2010. 4822

Mahowald, N. M., Muhs, D. R., Levis, S., Rasch, P. J., Yoshioka, M., Zender, C. S., and Luo, C.: Change in atmospheric mineral aerosols in response to climate: Last glacial period, preindustrial, modern, and doubled carbon dioxide climates, J. Geophys. Res., 111, D10202, doi:10.1029/2005JD006653, 2006. 4825, 4826, 4830

Maier-Reimer, E., Mikolajewicz, U., and Hasselmann, K.: Mean circulation of the Hamburg LSG OGCM and its sensitivity to the thermohaline surface forcing, J. Phys. Ocenogr., 23, 731–757, 1993. 4824

Mangini, A., Jung, M., and Laukenmann, S.: What do we learn from peaks of uranium and of manganese in deep sea sediments?, Mar. Geol., 177, 63–78, 2001. 4822, 4836

Moore, J. K. and Braucher, O.: Sedimentary and mineral dust sources of dissolved iron to the world ocean, Biogeosciences, 5, 631–656, doi:10.5194/bg-5-631-2008, 2008. 4822, 4824, 4825, 4828, 4829

Palastanga, V., Slomp, C. P., and Heinze, C.: Long-term controls on ocean phosphorus and oxygen in a global biogeochemical model, Global Biogeochem. Cy., 25, GB3024, doi:10.1029/2010GB003827, 2011. 4823, 4824, 4826, 4828, 4830

Parekh, P., Follows, M. J., and Boyle, E. A.: Decoupling of iron and phosphate in the global ocean, Global Biogeochem. Cy., 19, GB2020, doi:10.1029/2004GB002280, 2005. 4822, 4824, 4828, 4829

Raiswell, R.: Towards a highly reactive iron cycle, J. Geochem. Expl., 88, 436–439, 2006. 4825, 4826, 4830

Raiswell, R., Tranter M., Benning, L. G., Siegert, M., Death, R., Huybrechts, P., and Payne, T.: Contributions from glacially derived sediment to the global iron (oxyhydr)oxide cycle: Implications for iron delivery to the oceans, Geochim. Cosmochim. Acta, 70, 2765–2780, 2006. 4837

Ruttenberg, K. C.: Reassessment of the oceanic residence time of phosphorus, Chem. Geol., 107, 405–409, 1993. 4821, 4827, 4830, 4835

Schenau, S. J., Reichart, G. J., and de Lange, G. J.: Phosphorus burial as a function of paleoproductivity and redox conditions in Arabian Sea sediments, Geochim. Cosmochim. Ac., 69, 919–931, 2005.

BGD
9, 4819–4852, 2012

Sirocko, F., Garbe-Schonberg, D., and Devey, C.: Processes controlling trace element geochemistry of Arabian Sea sediments during the last 25 000 years, Global Planet. Change, 26, 217–303, 2000. 4822

Slomp, C. P. and Van Cappellen, P.: The global marine phosphorus cycle: sensitivity to oceanic circulation, Biogeosciences, 4, 155–171, doi:10.5194/bg-4-155-2007, 2007. 4822

Slomp, C. P., Epping, E. H. G., Helder, W., and Van Raaphorst, W.: A key role for iron bound phosphorus in authigenic apatite formation in North Atlantic continental platform sediments, J. Mar. Res., 74, 1179–1205, 1996. 4830

Tamburini, F. and Föllmi, K. B.: Phosphorus burial in the ocean over glacial-interglacial time scales, Biogeosciences, 6, 501–513, doi:10.5194/bg-6-501-2009, 2009 4821, 4835, 4836

Tamburini, F., Huon, S., Steinmann, P., Grousset, F. E., Adatte, T., and Föllmi, K. B.: Dysaerobic conditions during Heinrich events 4 and 5: evidence from phosphorus distribution in a North Atlantic deep sea core, Geochim. Cosmochim. Ac., 66, 4069–4083, 2002. 4822

Tamburini, F., Föllmi, K. B., Adatte, T., Bernasconi, S. M., and Steinmann, P.: Sedimentary phosphorus record from the Oman margin: new evidence of high productivity during glacial periods, Paleoceanography, 18, 1015, doi:10.1029/2000PA000616, 2003. 4836

Tsandev, I., Slomp, C. P., and Van Cappellen, P.: Glacial-interglacial variations in marine phosphorus cycling: Implications for ocean productivity, 22, GB4004, Global Biogeochem. Cy., doi:10.1029/2007GB003054, 2008. 4821

Tsandev, I., Rabouille, C., Slomp, C. P., and Van Cappellen, P.: Shelf erosion and submarine river canyons: implications for deep-sea oxygenation and ocean productivity during glaciation, Biogeosciences, 7, 1973–1982, doi:10.5194/bg-7-1973-2010, 2010. 4821, 4822, 4823, 4827, 4835, 4837

Tyrrell, T.: The relative influence of nitrogen and phosphorus on oceanic primary productivity, Nature, 400, 525–531, doi:10.1038/22941, 1999. 4820

Van Cappellen, P. and Wang, R. Y.: Cycling of iron and manganese in surface sediments: a general theory for the coupled transport and reaction of carbon, oxygen, nitrogen, sulfur, iron, and manganese, Am. J. Sci., 296, 197–243, 1996. 4826

Wallmann, K.: Feedbacks between oceanic redox states and marine productivity: A model perspective focused on benthic phosphorus cycling, Global Biogeochem. Cy., 3, 1084, doi:10.1029/2002GB001968, 2003. 4821, 4822, 4827, 4837

BGD
9, 4819–4852, 2012

Wijsman, J. W. M., Herman, P. M. J., Middelburg, J. J., and Soetaert, K.: A model for early diagenetic processes in sediments of the continental shelf of the Black Sea, Estuarine, Coastal and Shelf Science, 54, 403–421, 2002. 4826

Winguth, A. M. E., Archer, D., Duplessy, J. C., Maier-Reimer, E., and Mikolajewicz, U.: Sensitivity of paleonutrient tracer distributions and deep-sea circulation to glacial boundary conditions, Paleoceanography, 14, 304–323, 1999. 4826, 4837

BGD

9, 4819–4852, 2012

Table 1. Global fluxes of nutrients and particulate material in the preindustrial run (reference case) and the full LGM simulation.

Global fluxes	Reference case	Full LGM simulation
Input of dissolved nutrients		
Riverine PO_4	0.022 Tmol P yr^{-1}	0.022 Tmol P yr^{-1}
Atmospheric PO_4	0.003 Tmol P yr^{-1}	0.007 Tmol P yr^{-1}
Riverine Fe	0.0 mol Fe yr^{-1}	0.0 mol Fe yr^{-1}
Atmospheric Fe	1.5×10^9 mol Fe yr^{-1}	3.3×10^9 mol Fe yr^{-1}
Input of particulate P and Fe		
Authigenic Ca-P (dust and terrigenous[1])	0.008 Tmol P yr^{-1}	0.031 Tmol P yr^{-1}
Fe-oxides bound P (dust and terrigenous)	0.003 Tmol P yr^{-1}	0.014 Tmol P yr^{-1}
Organic P (terrigenous)	0.0 Tmol P yr^{-1}	0.04 Tmol P yr^{-1}
Detrital P (dust)	0.008 Tmol P yr^{-1}	0.012 Tmol P yr^{-1}
Highly reactive Fe or Fe-oxides (dust)	1.95 Tg yr^{-1}	4.57 Tg yr^{-1}
Highly reactive Fe or Fe-oxides (rivers)	3.8 Tg yr^{-1}	3.8 Tg yr^{-1}
Diagnosed fluxes of Fe into the sediment		
Deposition of Fe-oxides	52.8×10^9 mol Fe yr^{-1}	79.2×10^9 mol Fe yr^{-1}
Burial of Fe-oxides	42.2×10^9 mol Fe yr^{-1}	134.3×10^9 mol Fe yr^{-1}
Benthic release of Fe[2]	4.0×10^9 mol Fe yr^{-1}	7.4×10^9 mol Fe yr^{-1}

[1]Terrigenous fluxes from shelves are only implemented in the LGM simulation.
[2]The benthic release of Fe is prescribed using the function of Moore and Braucher (2008).

BGD
9, 4819–4852, 2012

Table 2. Fluxes of terrigenous POC and PP delivered into the continental slope and rise region ($200 < z < 2000$ m) for the model LGM scenario with input of terrigenous POC (LGM+POC), terrigenous inorganic P (LGM+PP), and both terrigenous POC and PP (full LGM).

Run	LGM+POC	LGM+PP	Full LGM
POC flux (TmolC yr^{-1})	5.0	0.0	5.0
total POC input (TmolC)[1]	6.0×10^5	0.0	6.0×10^5
total organic P input (TmolP)	0.05×10^5	0.0	0.05×10^5
PP flux (TmolP yr^{-1})	0.0	0.02	0.02
total PP input (TmolP)	0.0	0.024×10^5	0.024×10^5

[1] Total inputs of POC and P are calculated for a period of 120 kyr.

BGD
9, 4819–4852, 2012

Table 3. Glacial trends in total P burial (δP_{tot}) and reactive P burial (δP_{react}) from data and two sets of LGM simulations (LGM and full LGM).[1]

				Data			LGM simulation		Full LGM simulation	
Latitude	Longitude	Depth	Region	δP_{tot}	δP_{react}	Reference	δP_{tot}	δP_{react}	δP_{tot}	δP_{react}
−48.00	5.00	3636	SAO	+	+	[1]	+	+	+	+
−54.00	−5.00	2677	SAO	+	+		+	+	+	+
−45.00	106.00	3863	SIO	+	+		+	+	+	+
−41.00	10.00	4620	SAO	+	+	[2]	+	+	+	+
−53.00	5.00	2807	SAO	+	+		+	+	+	+
0.00	−139.00	4298	EPO	+	+		−	−	+	+
4.00	−140.00	4432	EPO	+	+		−	−	+	+
69.00	−12.00	1880	NAG	?	=	[3]	+	=	+	=
0.00	−160.00	2520	JP	−	−		−	−	+	+
20.75	−18.06	2263	ETA	+?	+		+	+	+	+
−11.00	−78.00	252	PEM	?	+		−	−	−	−
−17.75	57.60	293	OMM	+?	+		+	+	+	+
37.00	134.00	900	JAPS	?	+		+	+	+	+
18.05	57.08	593	OMM	N/A	+	[4]	+	+	+	+
23.05	66.00	1002	ARS	+	N/A	[5]	+	+	+	+
20.00	61.00	3570	ARS	+	N/A		+	+	+	+
22.07	−106.05	425	NWM	−	N/A	[6]	+	+	+	+

[1]Trends are categorized as “increase” (+), “decrease” (−), “unclear” (?), “unclear increase” (+?), and “no change” (=). Region abbreviations in the Region column are SAO for South Atlantic Ocean, SIO for South Indian Ocean, EPO for Equatorial Pacific Ocean, NAG for North Atlantic Gateways, JP for Java Plateau, ETA for Eastern Tropical Atlantic, PEM for Peru margin, OMM for Oman margin, JAPS for Japan Sea, ARS for Arabian Sea, and NWM for the waters off the Northwest Mexican coast. Index numbers for authors in the Reference column are [1] for Latimer and Filippelli (2001), [2] for Filippelli et al. (2007), [3] for Tamburini and Föllmi (2009), [4] for Tamburini et al. (2003), [5] for Schenau et al. (2005), and [6] for Ganeshram et al. (2002).

BGD
9, 4819–4852, 2012

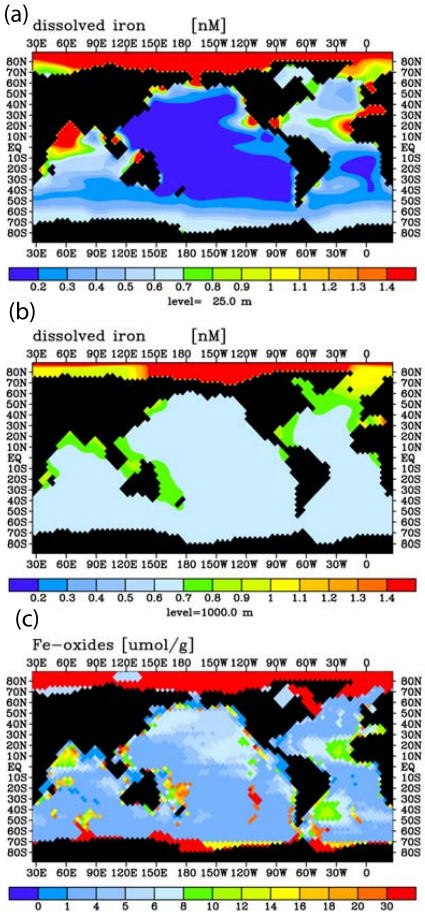

Fig. 1. Dissolved Fe concentrations (in nM) **(a)** in the surface ocean and **(b)** at 1000 m depth, and **(c)** Fe-oxide concentrations averaged over the sediment bioturbated layer (units in μmolFe g^{-1}), as simulated in the model reference run

BGD
9, 4819–4852, 2012

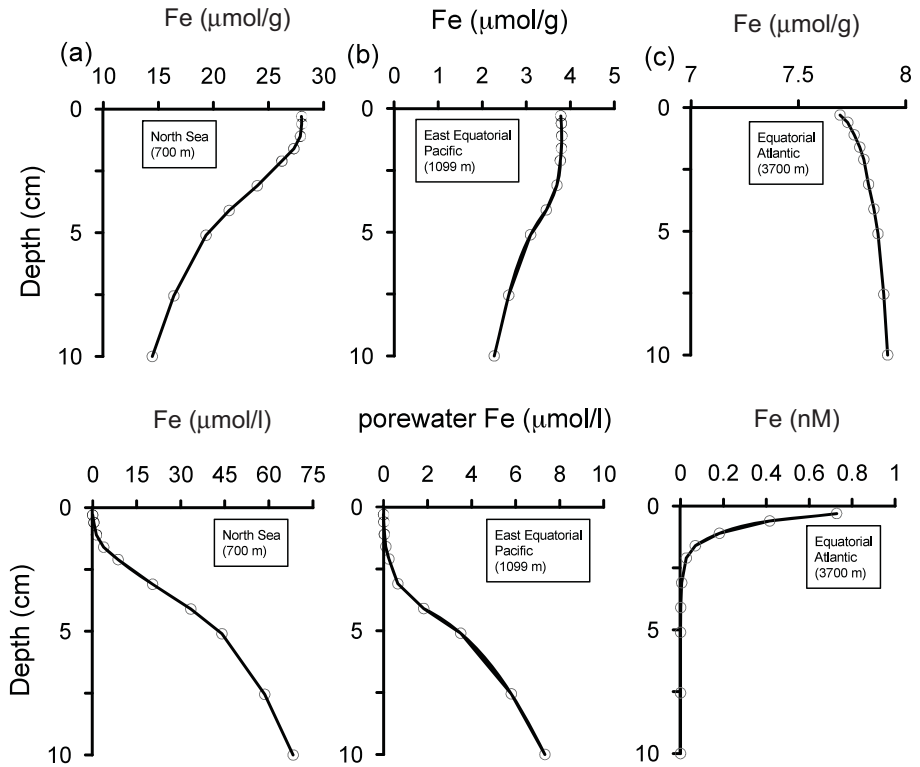

Fig. 2. Vertical profiles of Fe-oxides and porewater Fe in the sediment bioturbated layer at three locations in the **(a)** North Sea, **(b)** East Equatorial Pacific and **(c)** Equatorial Atlantic, as simulated in the model reference run.

BGD
9, 4819–4852, 2012

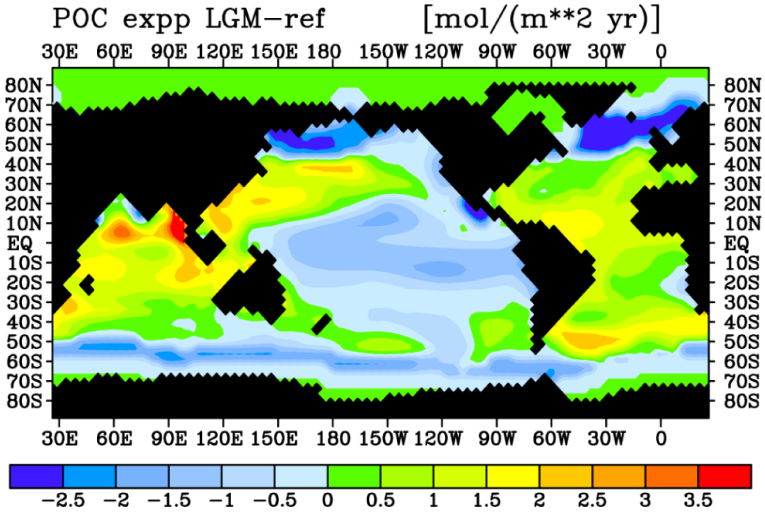

Fig. 3. Change in POC export production in the LGM simulation (without inputs of terrigenous material) relative to the reference run (units in mol m^{-2} yr^{-1}).

BGD
9, 4819–4852, 2012

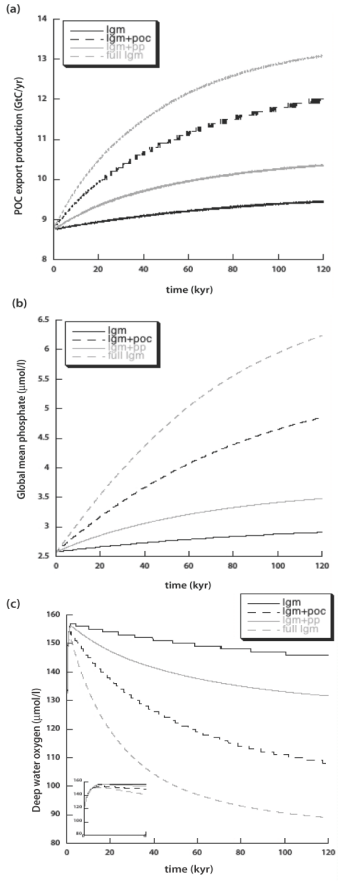

Fig. 4. Transient model response of **(a)** global POC export production, **(b)** global mean phosphate concentrations, and **(c)** mean oxygen concentrations at 1000 m depth, in the LGM simulation (black line; lgm), the LGM simulation with 5 TmolC yr^{-1} terrigenous POC (black dashed line; lgm+poc), the LGM simulation with 0.02 Tmol yr^{-1} terrigenous PP (grey line; lgm+pp), and the full LGM simulation (grey dashed line; full lgm). The inlet figure in **(c)** shows the oxygen variation in the first 6 kyr of the model simulations.

BGD
9, 4819–4852, 2012

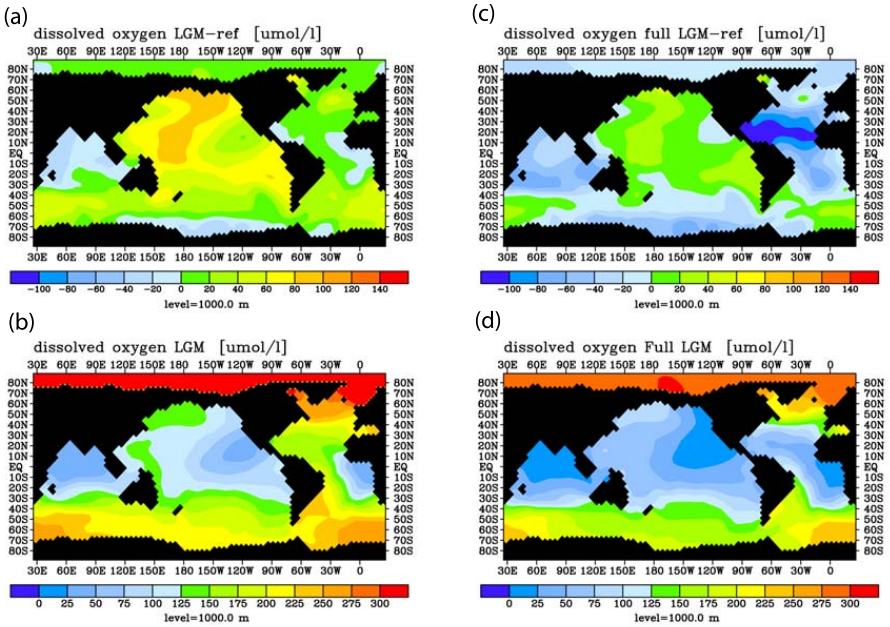

Fig. 5. Oxygen anomalies at 1000 m relative to the reference run in the model **(a)** LGM simulation and **(c)** full LGM simulation. Oxygen concentrations at 1000 m in the model **(b)** LGM simulation and **(d)** full LGM simulation. Units in μmol l^{-1}.

BGD
9, 4819–4852, 2012

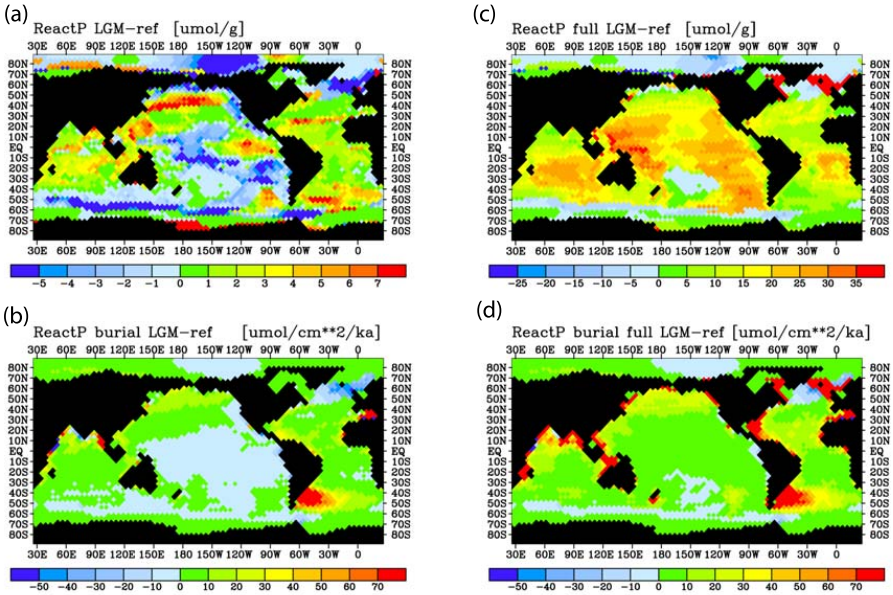

Fig. 6. Reactive P anomalies (averaged over the sediment bioturbated layer; units in μmolP g^{-1}) in the model **(a)** LGM simulation and **(c)** full LGM simulation, and reactive P burial anomalies (units in μmol cm^{-2} kyr^{-1}) in the **(b)** LGM simulation and **(d)** full LGM simulation, both relative to the reference run.

BGD
9, 4819–4852, 2012